

Journal of Materials Chemistry A

Accepted Manuscript



This is an *Accepted Manuscript*, which has been through the Royal Society of Chemistry peer review process and has been accepted for publication.

Accepted Manuscripts are published online shortly after acceptance, before technical editing, formatting and proof reading. Using this free service, authors can make their results available to the community, in citable form, before we publish the edited article. We will replace this *Accepted Manuscript* with the edited and formatted *Advance Article* as soon as it is available.

You can find more information about *Accepted Manuscripts* in the [Information for Authors](#).

Please note that technical editing may introduce minor changes to the text and/or graphics, which may alter content. The journal's standard [Terms & Conditions](#) and the [Ethical guidelines](#) still apply. In no event shall the Royal Society of Chemistry be held responsible for any errors or omissions in this *Accepted Manuscript* or any consequences arising from the use of any information it contains.



Journal Name

ARTICLE

One-step chemically controlled wet synthesis of graphene nanoribbons from graphene oxide for high performance supercapacitor applications

Received 00th January 20xx,
Accepted 00th January 20xx

DOI: 10.1039/x0xx00000x

www.rsc.org/

Mahima Khandelwal and Anil Kumar*

The present manuscript for the first time reports a novel one-step wet chemical approach to synthesize about 150-300 nm wide graphene nanoribbons (GNRs) by reduction of graphene oxide (GO) using malonic acid as a reducing agent. The optical, X-ray diffraction, high resolution transmission electron microscopy, Raman, Infrared, X-ray photoelectron spectroscopy and ^{13}C nuclear magnetic resonance (NMR) demonstrated the effective reduction of GO. The average thickness of GNRs has been estimated by atomic force microscopy at 3.3 ± 0.2 nm, which is reduced significantly to 1.1 ± 0.5 nm upon annealing at 300°C (GNRs-300). In the process of nucleation and growth, the intermediate(s), formed between the malonic acid and GO undergo twisting/folding involving supramolecular interactions to yield ~ 0.15 to 1 mm long curled GNRs. ^{13}C NMR demonstrates a significant increase in sp^2 character of nanoribbons following the order: GO < GNRs < GNRs-300 as was also evidenced by the conductivity measurements. GNRs exhibited high specific capacitance value of 301 F/g at 1 A/g with good cyclic stability for 4000 charge-discharge cycles at 15 A/g, and high energy density/power density (16.84 Wh/kg / 5944 W/kg) in aqueous electrolyte demonstrating their tremendous potential as electrode material for energy storage applications.

Introduction

Graphene (2D) has become one of the most explored carbonaceous materials because of its emerging new applications in the areas of electronics, electrical, mechanical, electrochemical and biotechnology.¹⁻⁵ The graphene based materials are drawing increasing attention for their usage in energy storage devices as supercapacitor because of their conducting nature and high surface area.^{6,7} It is very attractive and challenging to control the dimensionality of graphene chemically, as it would provide a novel tool to tailor the characteristic features of these materials. In recent years synthesis of graphene nanoribbons (GNRs) has been considered to be of significant importance because of their high aspect ratio with the increased edges, more prone to easy functionalization and allowing precise control of their electronic properties. These materials have attracted wide attention due to their potential in electrocatalytic activity and electronic devices, and as electrode materials.⁸⁻¹⁰ In literature, covalent and non-covalent approaches have been explored for the functionalization of graphene.¹¹ The covalent approach often disturbs the extended sp^2 conjugation of graphene causing a reduction in the electronic properties. For this reason, non-covalent functionalization of graphene offers better approach for the functionalization without disturbing the electronic structure.

A number of methods have been employed for the

synthesis of GNRs like lithographic patterning of graphene,^{12,13} sonochemical cutting of graphene sheets,¹⁴ chemical vapour deposition,^{15,16} longitudinal unzipping of carbon nanotubes (MWCNTs),¹⁷⁻¹⁹ metal-catalyzed²⁰ and chemical method.²¹⁻²⁴ We have come across only one research article employing the wet chemical route for the synthesis of GNRs by the reduction of GO using fairly high concentration of NaOH as reductant having a width of ~ 10 μm . It involved five steps of synthesis followed by heating at varied temperatures ranging from $100 - 800^\circ\text{C}$.²⁵ The reduction of GO has lately been reported to be susceptible to various factors such as concentration of the reducing agent, pH and temperature.^{26,27}

In the present work, we have employed for the first time a one-step chemically controlled wet synthesis of GNRs by the reduction of GO using malonic acid as a reducing agent. Specifically, the concentration(s) of malonic acid and the pH of the medium have been explored to optimize the process of reduction of GO as regards to the controlled nucleation and growth of graphene with desired dimensionality. At mild concentration of malonic acid (1.6 mg/mL) and low pH (~ 6.0) of the reaction mixture, the initial growth of graphene sheet(s) upon folding produces nanoribbons, whereas at higher pH ($> 8 - 11$) and higher concentrations ($> 2.6 - 3.6$ mg/mL) nanosheets are obtained. Interestingly, it presents a novel method demonstrating the tremendous effect of pH to bring a change in the morphology of carbon nanostructures involving supramolecular interactions.

The as synthesized GNRs show fairly high conductivity and specific capacitance value, long-term cyclic stability at high current density (15 A/g). It also exhibited high coulombic efficiency and energy density / power density. All these features suggest the potential of this material for high performance supercapacitor.

Department of Chemistry, Indian Institute of Technology Roorkee, Roorkee-247667, India. E-mail: anilkfcy@iitr.ac.in; akmshfcy@gmail.com; Fax: +91 1332 273560; Tel: +91 1332 285799

† Electronic Supplementary Information (ESI) available: See DOI: 10.1039/x0xx00000x

Results

Optical studies

Fig. 1 presents the optical absorption spectra of precursor GO and reduced graphene oxide (rGO), obtained by the reduction of GO at pH 6.0 using malonic acid as reductant. The absorption spectrum of GO exhibits a peak at 231 nm and a shoulder at 303 nm, which can be attributed to $\pi-\pi^*$ transition due to C=C bonds and $n-\pi^*$ transition due to C=O bonds, respectively (Fig. 1A-a). On the contrary, the absorption spectrum of rGO shows a red shifted broad absorption band peaking at 262 nm after 10 h of reduction (Fig. 1A-b). Digital photographs of GO and rGO obtained by dispersing them in water at pH 6.0 are shown in Fig. 1A- Inset. The appearance of dark black color in vial 'b' compared to that of yellowish - brown color in vial 'a' clearly indicates the effective reduction of GO possibly yielding graphene. After 10 h of reaction, there is no shift in the absorption peak of the product was observed (Fig. 1B). This indicates that the conjugated structure was restored upon reduction of GO. The time dependent variation in the optical absorption spectra of GO as a function of heating time up to 10 h is shown in Fig. 1C.

The stability of the colloidal dispersion of rGO was examined by performing dynamic light scattering measurement of rGO. The ζ -potential of this dispersion was found to be - 45.1 mV suggesting it to be fairly stable (Fig. S1, ESI[†]).

X-ray diffraction (XRD) analysis

The XRD patterns of graphite, GO, rGO and its annealed sample at 300 °C (rGO-300) are shown in Fig. 2. The XRD pattern of graphite shows a sharp peak corresponding to the reflection from (002) plane at 26.2° with the 'd' spacing of 0.339 nm (Fig. 2a). Whereas, GO exhibits slightly broader peak at 10.59° with the 'd' spacing of 0.835 nm matching to the reflection from (002) plane (Fig. 2b). These patterns are very similar to those reported earlier for graphite and GO.²⁶ The XRD pattern of rGO is quite different to those of precursors, graphite and GO, and shows a broader peak at 24.74° which corresponds to the reflection from (002) plane with the 'd' spacing of 0.360 nm clearly indicating the reduction of GO (Fig. 2c). In contrast to XRD pattern of rGO, rGO-300 shows a relatively sharper peak at 25.2° again corresponding to the reflection from (002) plane with the 'd' spacing of 0.353 nm (Fig. 2d). The reduction in the value of 'd' spacing from 0.360 nm (rGO) to 0.353 nm (rGO-300) suggests that the crystallinity of rGO is increased upon annealing at mild temperature.

Atomic force microscopy (AFM) analysis

AFM was used to characterize the topography of GO and rGOs and to determine their surface heights. The AFM image of GO shows the presence of about 1.4 nm thick sheets suggesting it a single layer as reported in previous studies²⁸ (Fig. 3a and a'). The reduction of GO under the used experimental conditions resulted in the formation of graphene nanoribbons (GNRs).

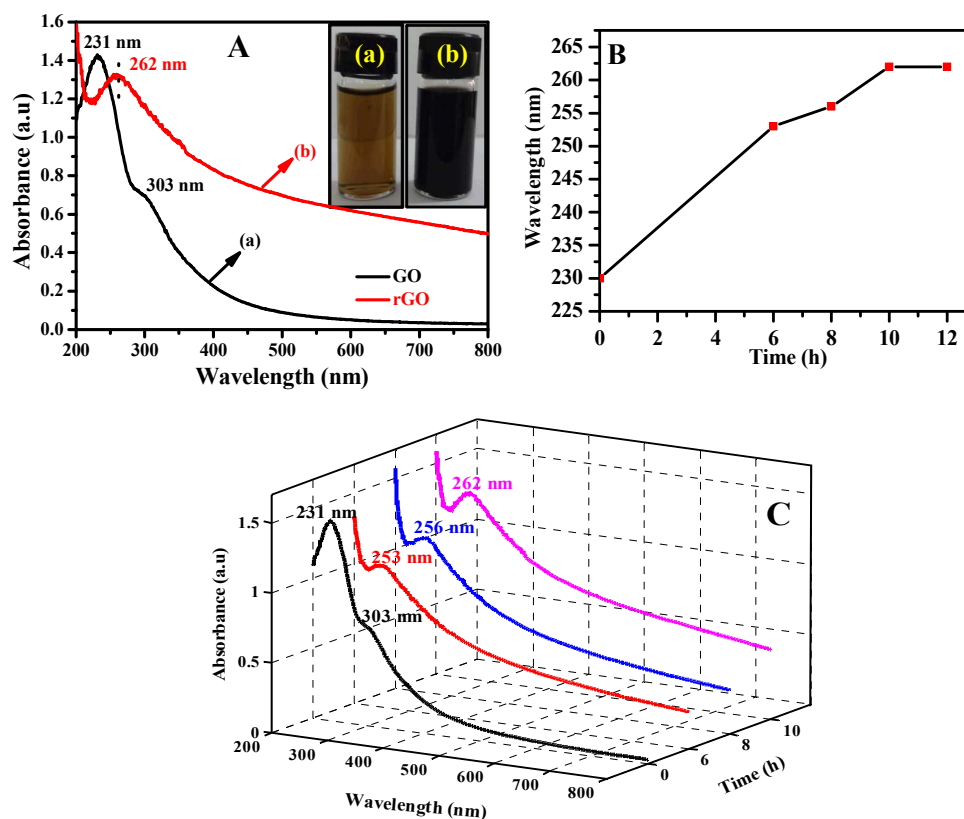


Fig. 1 Optical absorption spectra of GO (a) and rGO (b) along with their digital photographs captured by dispersing them in water – Inset – (panel A). A shift in the absorption maximum of GO with the heating time – (panel B). Optical absorption spectra of GO changing as a function of heating time up to 10 h – (panel C).

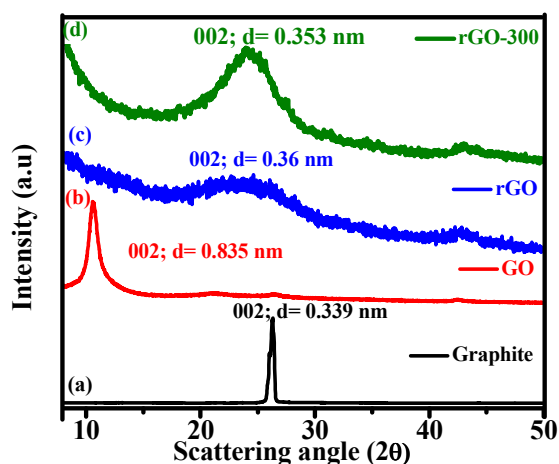


Fig. 2 XRD patterns of graphite (a), GO (b), rGO (c) and rGO-300 (d).

The surface height of these nanoribbons, analyzed at several locations by recording the line profile, was found to be 3.3 ± 0.2 nm (Fig. 3b and b'). However, the surface height of GNRs, monitored for several such synthesized samples, was computed to be 3.0 ± 0.5 nm. These data evidently suggest that the nanoribbons are produced by folding of rGO to a few layers. The 2D images of GNRs annealed at 300°C (GNRs-300) are shown in Fig. 3c and c'. Line profile analysis of a small portion of the image (Fig. 3c') is shown in Fig. 3c''. The average height of these nanoribbons was computed to be 1.1 ± 0.5 nm, which indicates them to contain 3 to 4 layers.

Field emission scanning electron microscopy (FE-SEM) analysis

The morphologies of the precursor GO and the products GNRs and its annealed sample at 300°C (GNRs-300) have been examined using FE-SEM (Fig. 4). The EDAX spectra of the FESEM image(s) were recorded at the location(s) marked by (+) sign in red. The FESEM image of GO shows it to contain the agglomerated sheet like structure (Fig. 4a). EDAX analysis of this sheet at the location marked by (+) sign shows the C/O ratio to be of the order of 1.59 (Fig. 4a'). The elemental mapping for the small area of this sheet shows the homogeneous distribution of carbon and oxygen (Fig. S2, ESI[†]). On the other hand, the FESEM images of the reduction product of GO, recorded at both lower and higher magnifications, shows the formation of nanoribbons like morphology (Fig. 4b and b'). The curl shaped nanoribbons are entangled with each other exhibiting their multiple folding, and for this reason it was not possible to determine the width and length of individual nanoribbons accurately. However, from some of the FESEM images captured at low resolutions, the length of these curled nanoribbons was estimated to vary in the range from 0.15 to 1 mm (Fig. S3, ESI[†]). EDAX analysis of these nanoribbons, recorded at higher magnification, shows C/O ratio to be 6.05 (Fig. 4b''), which is more than 3 times to that of GO (1.59) indicating the effective reduction of GO. This observation is also supported by the elemental mapping of another image of GNRs recorded at lower magnification, which showed the homogeneous distribution of carbon and oxygen with a much higher density for carbon (Fig. S4, ESI[†]). On the other hand, the morphology of GNRs-300 reveals more of the unfolding of the

GNRs with the higher C/O ratio (Fig. 4c and c'). A comparison of the EDAX analysis of these samples exhibits C/O ratio to increase in the following order: GO (1.59) < GNRs (6.05) < GNRs-300 (8.21).

Transmission electron microscopy (TEM) analysis

Fig. 5 shows the TEM images of GO, GNRs and GNRs-300 along with their SAED patterns and EDAX spectra. TEM image of GO reveals the formation of sheet like structure (Fig. 5a). Its SAED pattern shows it to be polycrystalline and corresponds to the planes (101) and (110) of graphite having a hexagonal structure matching with the JCPDS file no. 75-1621, very similar to that reported earlier²⁶ (Fig. 5a – Inset). On the other hand, the TEM image of GNRs clearly shows the formation of coiled nanoribbons. These nanoribbons were observed to have the width ranging from about 150–300 nm as was estimated from several such TEM images of GNRs prepared at different times (Fig. 5b).

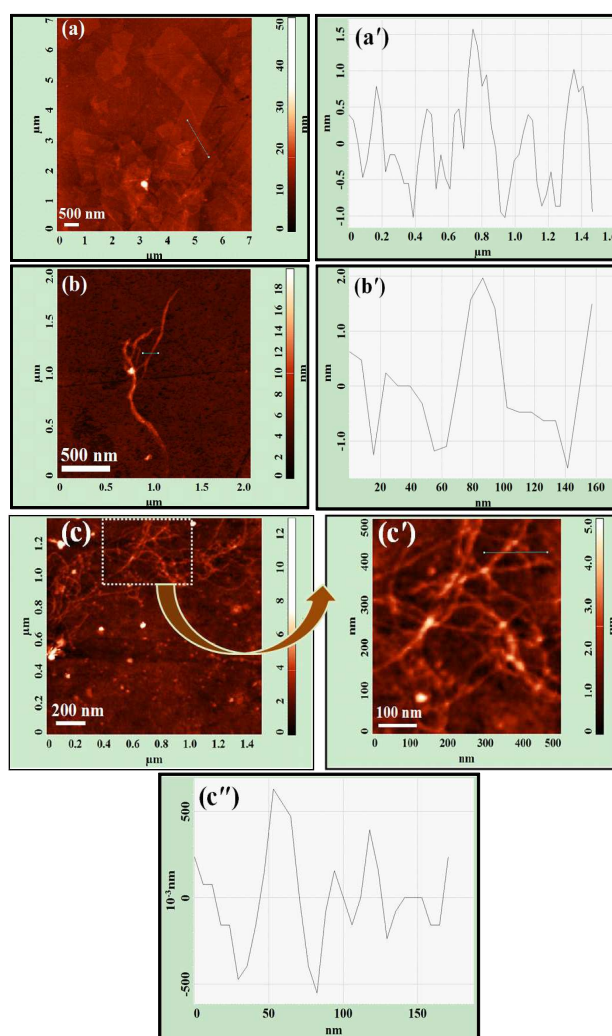


Fig. 3 AFM images and their height profile along a particular line: GO (a, a'), GNRs (b, b') (the surface height of GNRs at the typical indicated location measured by its line profile comes out to be 3.15 nm); GNRs-300 image at lower and higher magnifications (c, c') and its height profile along a particular line (c'').

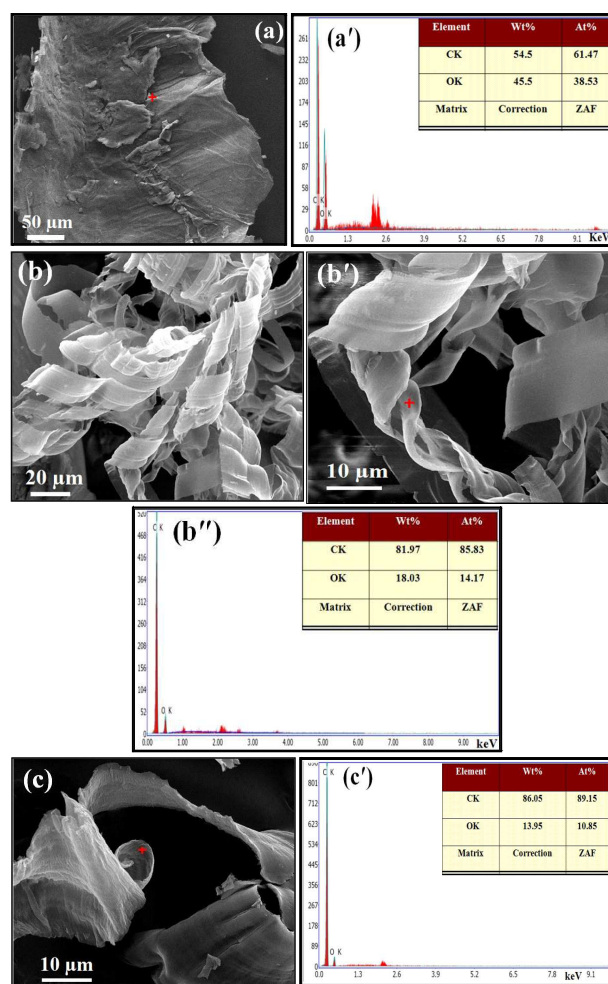


Fig. 4 FE-SEM images and their EDAX analysis on a particular location marked by (+) sign in red: GO (a, a'), GNRs (b, b', and b''), and GNRs-300 (c, c'), respectively.

Its SAED pattern shows diffused concentric rings corresponding to the planes (101) and (110) (Fig. 5b – Inset), indicating the amorphous nature. HRTEM analysis of this sample did not show any fringes. Annealing of GNRs at a mild temperature of 300 °C (GNRs-300) produces more of unfolded nanoribbons as is revealed by its images recorded at lower and higher magnifications (Fig. 5c and c'). Unlike GNRs, GNRs-300 shows relatively smaller width ranging from about 140–200 nm. SAED analysis of GNRs-300, however, exhibits the polycrystalline nature displaying ring pattern containing largely binary and ternary spots, thereby, indicating it to arise from bilayer and trilayer GNRs (Fig. 5c''). EDAX analysis of these samples exhibits the C/O ratio to increase in the order of: GO < GNRs < GNRs-300 (Fig. 5a', b' and c''). In case of GNRs-300 we could, however, obtain the lattice fringes suggesting its polycrystalline nature (Fig. 5c'''). From these fringes the number of layers could be counted at different locations. Multiple layers at places were stacked on each other, appearing as bundles and entangled with each other very similar to that seen in AFM image for this sample (Fig. 3c and c'). The locations where there was no entanglement, it exhibited the presence of 3–4 layers, which matches well with the observations made from its AFM analysis (Fig. 3), but at the locations where entanglement was evident the number of layers were found to vary

from 10–24 layers (Fig. 5c'''). The average 'd' spacing from these fringes were estimated to be 0.35 ± 0.01 nm (Fig. 5c''''- Inset), and this value matches fairly well with the previous report on GNRs in which GNRs were produced by the pyrolysis of the solvothermal product obtained from propanol and sodium²¹, as well as with the XRD data (Fig. 2). The observation about the number of layers upon annealing in the GNRs-300, is, however, more evident from the AFM images, where it could become possible to observe the surface height of individual nanoribbon (Fig. 3 c'').

Brunauer–Emmett–Teller (BET) surface area analysis

In view of the reduced thickness and difference in the morphologies of as synthesised GNRs and GNRs-300, N₂ sorption isotherms were performed in order to obtain BET specific surface area and pore structure of these nanoribbons (Fig. S5, ESI†). For both the samples (GNRs and GNRs-300), type IV isotherms were observed with the hysteresis loop according to International Union of Pure and Applied Chemistry (IUPAC) classification. From these measurements the average pore diameter (pore size distribution) for GNRs and GNRs-300 was found to be: 1.9 nm (1.6 – 4.6 nm) and 4.0 nm (3.2 – 8.4 nm), suggesting them to be microporous and mesoporous, respectively. As expected the GNRs-300 has a BET specific surface area of 470 m²/g which is more than 3 times to that of GNRs (129 m²/g). This is also evidenced by the reduced thickness for GNRs-300 measured by AFM analysis (Fig. 3).

Infrared (IR) analysis

IR spectra of GO, GNRs and GNRs-300 were recorded in the mid IR range (4000 - 500 cm⁻¹) in order to verify the reduction of GO (Fig. 6). The IR spectrum of GO shows bands (cm⁻¹) at: 3423, 1727, 1631, 1223, and 1054, which have been assigned to –OH stretching, C=O (COOH), C=C, C-O-C (epoxy) and C-O (alkoxy), respectively and matches with the previous report²⁹ on GO. The IR spectrum of GNRs was fairly different to that of GO in which the intensity of peaks (cm⁻¹) due to: –OH (3431), C=O (1745) and C-O (1093) are reduced along with a slight blue shift and the peak due to C-O-C (1223) has vanished completely. Apart to this, the bands due to symmetric and asymmetric stretching of C-H at 2923 and 2857 cm⁻¹ have become fairly intense and the peak due to C=C is still retained. These observations suggest that the reduction of GO has been largely effective but still contains some residual functionalities on GNRs. The IR spectrum of GNRs-300 showed further reduction in the intensity of peaks due to –OH stretching and C-O (alkoxy), and the peak due to C=O (COOH) is almost vanished. Whereas, the bands due to symmetric and asymmetric stretching of C-H and the peak due to C=C are still retained. From these findings, it is evident that sp² character is significantly enhanced for both GNRs and GNRs-300 as compared to that of GO. Specifically, in case of GNRs-300 the residual oxygen functionalities have reduced to a greater extent.

Raman analysis

The electronic structure of graphite, GO, GNRs and GNRs-300 were examined by Raman spectroscopy (Fig. 7) and these spectral data have been summarized in Table S1, ESI†. The Raman spectra of graphite and GO exhibit the spectral features very similar to those reported previously^{26,30} (Fig. 7A - a and b). A careful analysis of the Raman spectra of GNRs reveals its I_D/I_G ratio to be 0.97 which is higher to that of GO (0.88) (Fig. 7A - c) indicating the reduction of GO. Moreover, an additional D' band is noted at 1623 cm⁻¹ in GNRs (Fig. 7C - c''). The annealing of this sample at mild temperature of 300 °C (GNRs-300) results in the decrease in the intensity of D band associated with the decrease in I_D/I_G ratio to 0.94 along with the

elimination of the D' band (Fig. 7A - d and 7C - d''). Moreover, G band is red shifted (Fig. 7B - d'). These features indicate an increase in the structural order in GNRs-300.

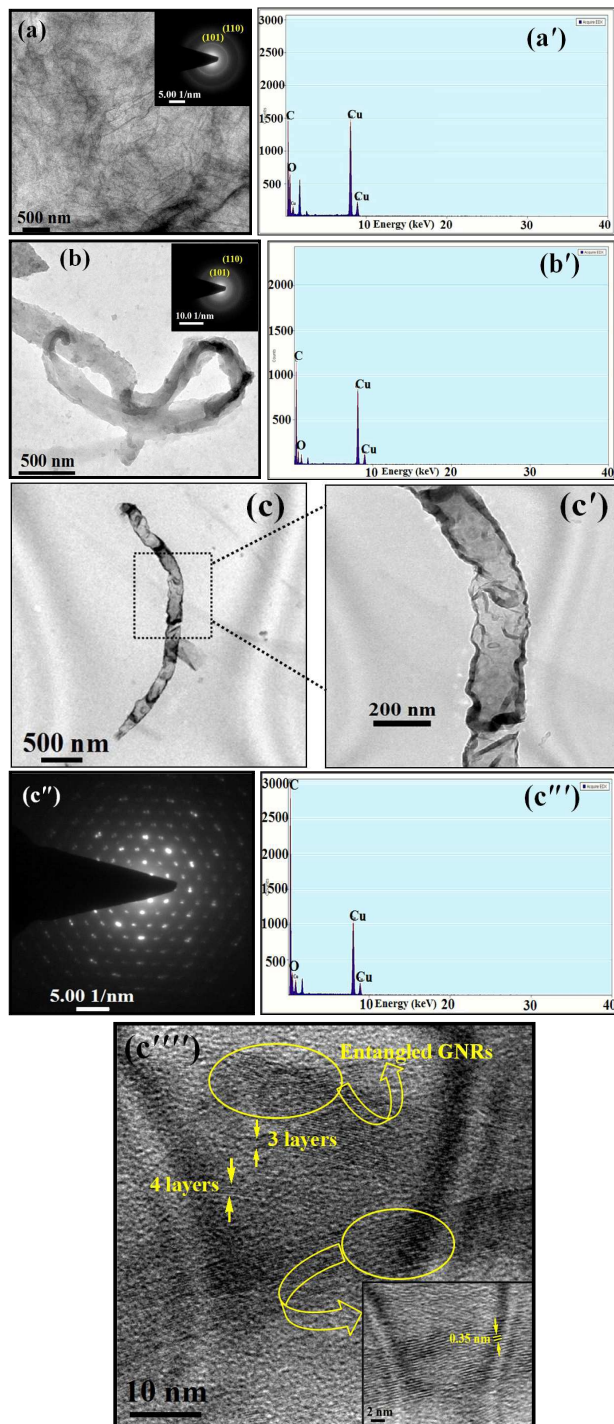


Fig. 5 TEM images containing SAED patterns shown in the inset and their EDAX analysis: GO (a, a') and GNRs (b, b'). TEM images of GNRs-300 at lower (c) and higher magnifications (c'). SAED pattern (c'') and EDAX analysis (c''') of GNRs-300. HRTEM image of GNRs-300 (c''') and its magnified image showing the 'd' spacing (Inset - c''').

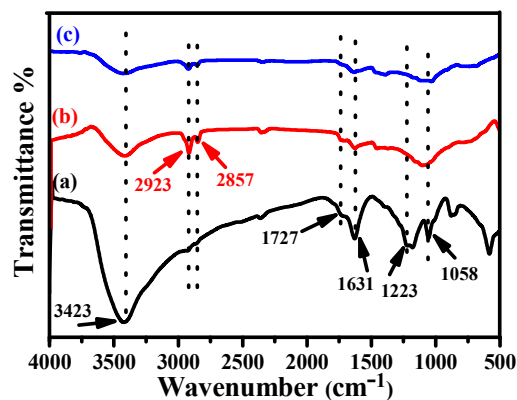


Fig. 6 FTIR spectra of: GO (a), GNRs (b) and GNRs-300 (c).

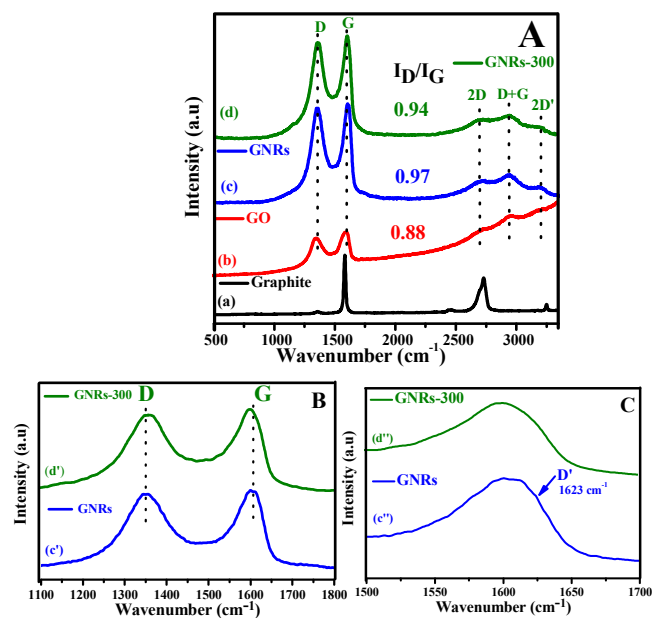


Fig. 7 Raman spectra of: graphite (a), GO (b), GNRs (c) and GNRs-300 (d) – (panel A); Expanded Raman spectra of: GNRs (c') and GNRs-300 (d') in 1100-1800 cm^{-1} range – (panel B). D' band of: GNRs (c'') and GNRs-300 (d'') in 1500-1700 cm^{-1} range – (panel C).

X-ray photoelectron spectroscopy (XPS) analysis

The survey scans for the surface analysis of GO and GNRs performed by using XPS are shown in Fig. 8A. An examination of these spectra reveals that C/O ratio is significantly increased in GNRs as compared to that of GO (Fig. 8A). The high resolution C 1s spectrum of GO consists of four different components of carbon, C=C bonds contributed by the sp^2 aromatic structure (284.2 eV), C-C from sp^3 hybridised carbon/C-OH from hydroxyl (286.1 eV), C-O from epoxy/alkoxy (286.8 eV) and C=O from carboxyl group (288.1 eV) as observed earlier.²⁶ In contrast to GO, C 1s spectrum of GNRs exhibits three different components of carbon arising from C=C (284.2 eV), C-C/C-OH (286.1 eV) and C=O (288.1 eV). Moreover, the intensity due to C=C component is enhanced, whereas, due to C-C/C-OH is reduced. The high resolution O 1s spectrum due to GO shows three different components of oxygen at a binding energy (eV) of: 529.8, 531.4 and 532.5, which have been assigned to lattice oxygen, carbon double bonded to oxygen (C=O) and carbon single

bonded to oxygen (epoxide and hydroxyl), respectively. In case of GNRs, O 1s spectrum also exhibits three different components of oxygen at a binding energy (eV) of: 531.8, 533.2 and a broad peak at 535.0, which have been attributed to carbon double bonded to oxygen (C=O), physisorbed water and due to charging effect, respectively.^{31,32} Further, a comparison of O 1s spectra of GO and GNRs in panel D and E clearly shows that the intensity due to O 1s band is reduced by about 2 fold in case of GNRs. These data clearly indicate the reduction of GO into GNRs.

Solid state ¹³C-NMR

The reduction of GO into GNRs was further examined by recording solid state ¹³C magic angle spinning (MAS) NMR spectra of GO, GNRs and GNRs-300 (Fig. 9). The NMR spectrum of GO shows the

presence of five different components of carbon (chemical shift (approx.) in ppm) namely, C-O-C (61), C-OH (70), graphitic sp² carbon (100-140), O-C=O carbonyl carbon of ester (167) and ketonic C=O group (190), which are similar to those reported earlier in the literature.³³ In contrast to GO, the NMR spectrum of GNRs exhibits almost complete elimination of the carbon component due to C-O-C and ketonic C=O and a tremendous decrease in the intensity of the peaks due to C-OH and O-C=O. Further, ¹³C MAS NMR spectrum of GNRs-300 exhibits the elimination of all the functionalities: C-O-C, C-OH, O-C=O and C=O. Interestingly, the reduction of GO into GNRs results in the enhancement of the broad resonance peaks due to graphitic components (100-140 ppm) and follows the order: GO < GNRs < GNRs-300, suggesting the increasing graphitic (sp²) character of the as synthesized nanoribbons.

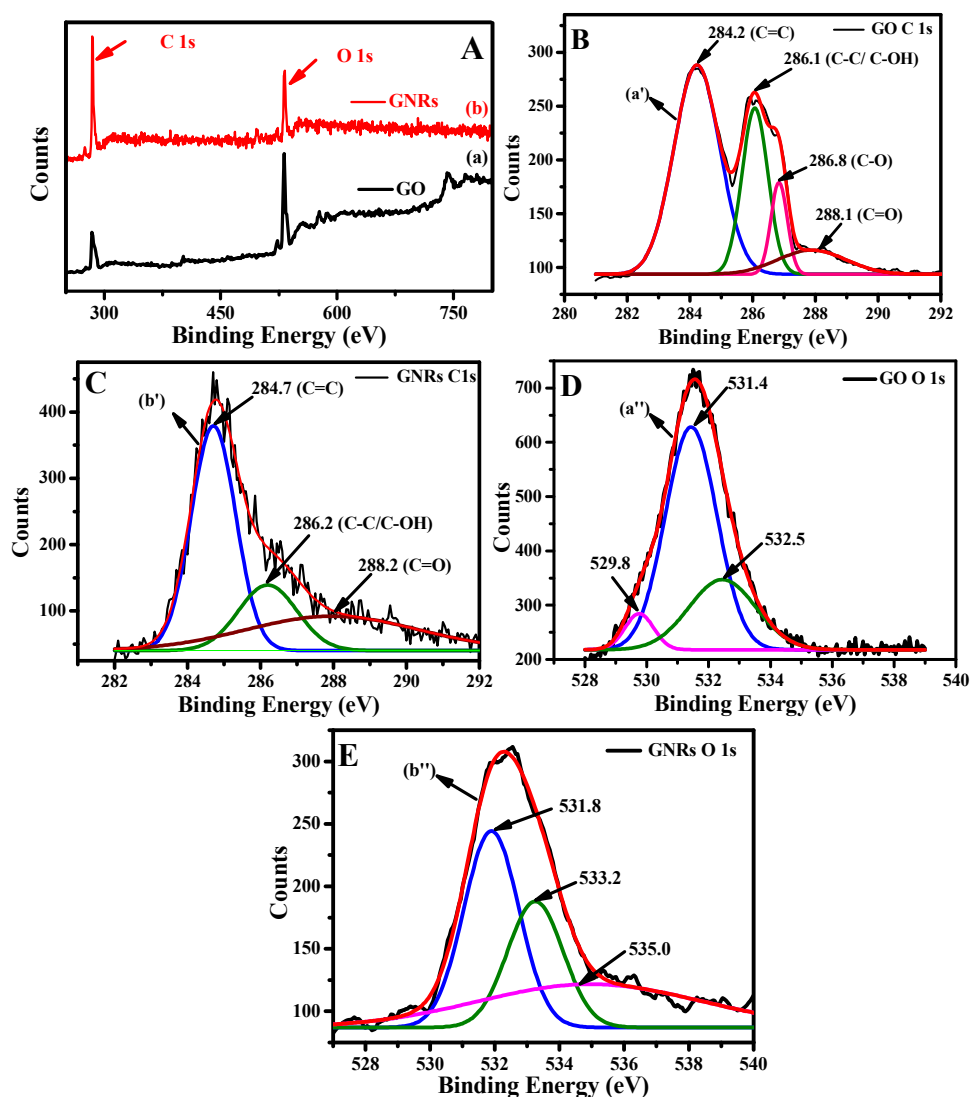


Fig. 8 XPS survey scans of: GO (a) and GNRs (b) – (panel A); GO C 1s (a') – (panel B); GNRs C 1s (b') – (panel C); GO O 1s (a'') - (panel D) and GNRs O 1s (b'') - (panel E).

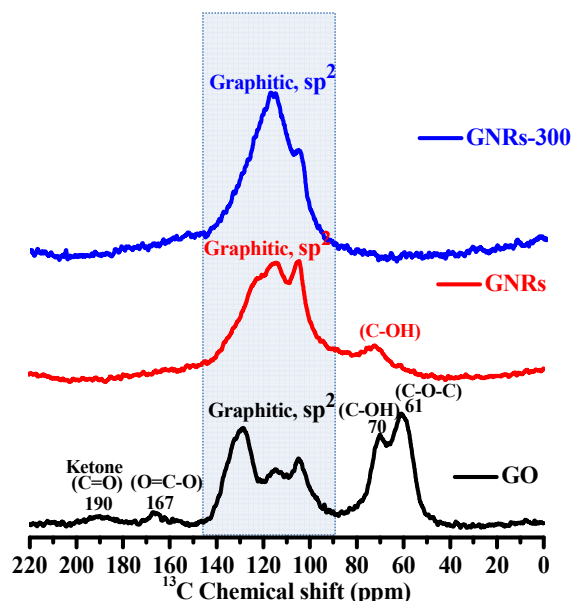


Fig. 9 Solid state ^{13}C magic-angle spinning (MAS) NMR spectra of GO, GNRs and GNRs-300 at 12 kHz.

Current-Voltage (I-V) measurements

In order to ascertain the extent of reduction of as synthesized GNRs, I-V profiles were recorded for all the samples, GO, GNRs and GNRs-300 (Fig. 10). I-V curve for GO shows the conductivity value of 2.7×10^{-4} S/cm, whereas, the values of conductivity for GNRs and GNRs-300 increased significantly to 2.85 S/cm and 14.7 S/cm, respectively.

Electrochemical measurements

The electrochemical characteristics of GO, GNRs and GNRs-300 as an electrode material were investigated for the supercapacitor application (Fig. 11). Cyclic voltammetry (CV) curves of GO, GNRs and GNRs-300 at different scan rate(s) ranging from 5 to 100 mV/s were recorded in the voltage range of 0.0 to 0.8 V. These curves exhibited an increase current density with increasing scan rates (Fig. 11A-C). The values of specific capacitance (C_s (F/g)) for GO, GNRs and GNRs-300 at the scan rates of 5, 10, 30, 50, 70 and 100 mV/s were calculated to be: 2.02, 1.65, 1.27, 1.12, 1.04 and 0.96; 210, 189, 161, 145, 134 and 122; and 185, 147, 121, 113, 99 and 91, respectively (Fig. 11A-D). For a typical scan rate of 100 mV/s, the C_s value for GNRs (122 F/g) and GNRs-300 (91 F/g) are much higher as compared to that of GO (0.96 F/g) (Fig. 11E). The lower value of C_s of GO electrode as compared to that of GNRs and GNRs-300 may be attributed to the poor conductivity of GO (Fig. 10). This observation is also supported by sp^3 hybridisation and low faradic rate of reaction in GO besides its lower surface area ($38.9 \text{ m}^2/\text{g}$). Interestingly, the CV curves for GNRs were almost rectangular in shape with a small redox hump suggesting it to have major contribution arising from electrical double layer capacitor (EDLC) and a minor contribution from the pseudo-capacitance due to the residual functionalities similar to those reported earlier.^{34,35} Whereas, in case of GNRs-300 the shape of the CV curve was almost rectangular unlike to that of GNRs indicating the elimination of

residual functionalities largely upon annealing at mild temperature of 300 °C.

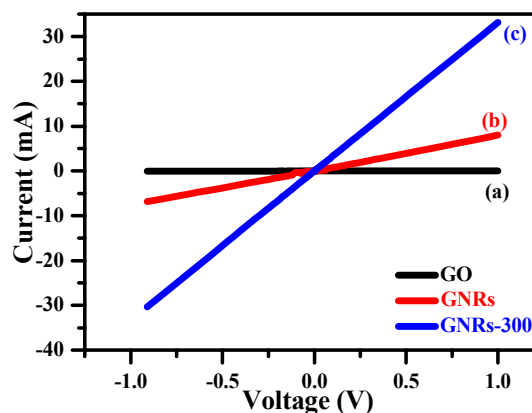


Fig. 10 I-V curves of GO (a), GNRs (b) and GNRs- 300 (c).

The electrochemical capacitive performance for GO, GNRs and GNRs-300 as electrode materials was also determined by galvanostatic charge-discharge (GCD) measurements in the same potential range of 0.0 to 0.8 V as was used for CV measurements. Fig. 11F and G shows the charge-discharge curves for GNRs and GNRs-300 at various current densities: 1, 2, 3, 5, 7, 10 and 15 A/g from which the C_s values (F/g) were calculated to be 301, 263, 250, 237, 230, 227 and 193, and 247, 220, 205, 186, 174, 163 and 149, respectively. The shape of these curves is nearly symmetrical triangle. The variation in the current density from 1 to 15 A/g results in the reduction of C_s values for GNRs and GNRs-300 from 301 to 193 F/g and 247 to 149 F/g (Fig. 11H). It is worth noting that even at the high current density of 15 A/g, the value of C_s for GNRs and GNRs-300 is fairly high. For comparison purpose the GCD curves for GO and GRH (obtained by the reduction of GO using malonic acid in the present work, *vide infra*) (not shown) were also recorded at 1 A/g and the values of C_s were calculated to be 2.5 F/g and 220 F/g, respectively. The value for GO is considerably lower to that of GNRs (301 F/g at 1A/g) and GNRs-300 (247 F/g at 1A/g) (Fig. 11I). Notably, the C_s value even for GRH is fairly lower as compared to those of GNRs and GNRs-300.

For GNRs, the long term cycling stability was examined for 4000 cycles at the highest used current density (15 A/g) (Fig. 11J). The typical portions of these runs exhibiting the first three and last three cycles are shown in Fig. 11J- inset. The C_s for the first cycle was observed to be 193 F/g, which remains constant up to about 80 cycles and is increased gradually to 210 F/g up to 4000th cycle. This increase in the value of C_s after 80th cycle may be attributed to the residual functionalities on GNRs (Fig. 6). Similar observations have been made about the role of residual functionalities in previous studies.^{35,36} For 4000 cycles, charging – discharging curve recorded at 15 A/g, exhibited the coulombic efficiency of 100 % (Fig. 11J).

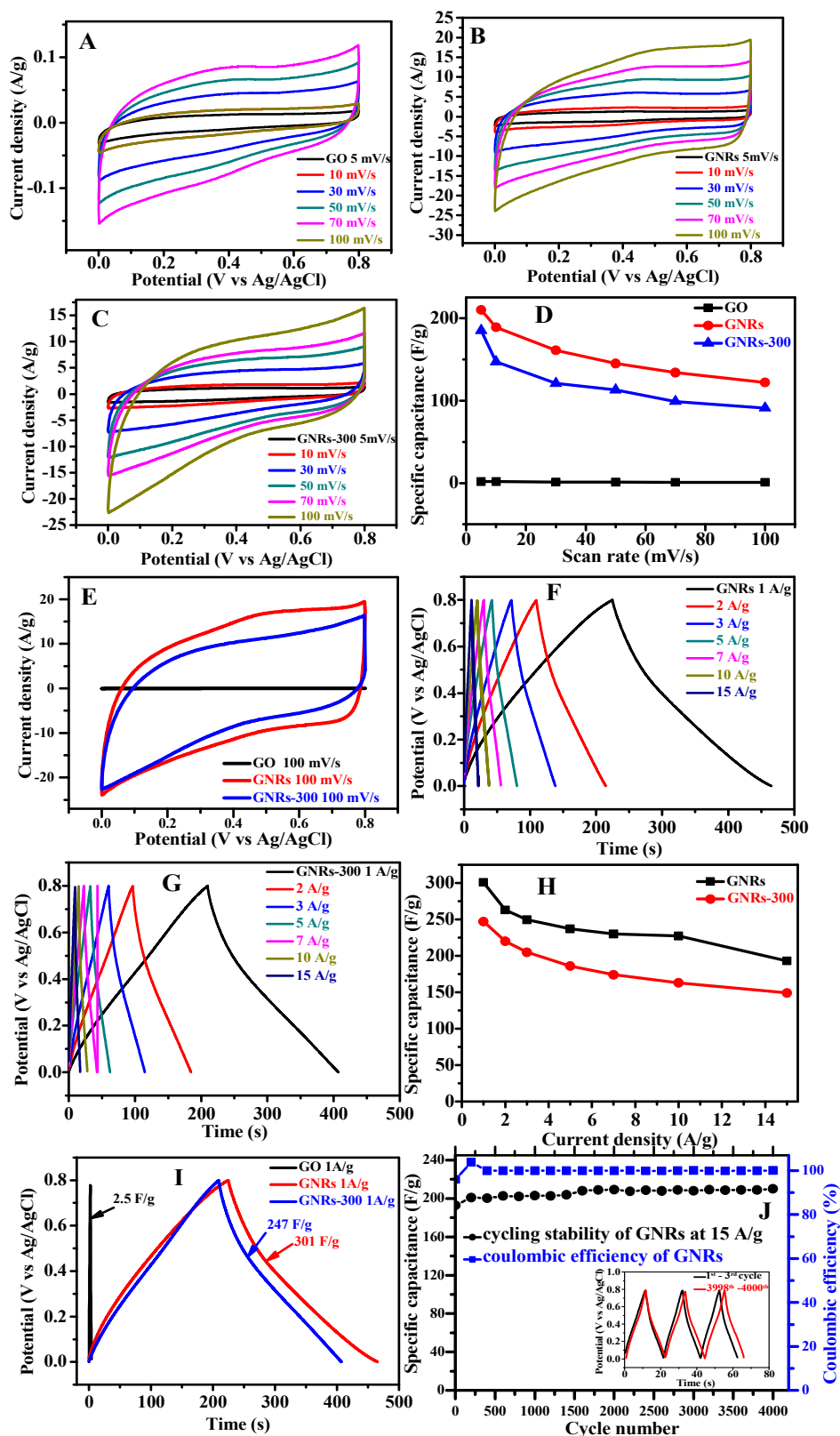


Fig. 11 CV curves of GO, GNRs and GNRs-300 at different scan rates – (panels A, B and C). Variation in the value of specific capacitance (C_s) as a function of scan rate for: GO, GNRs and GNRs-300 – (panel D). A typical CV curve of GO, GNRs and GNRs-300 at a scan rate of 100 mV/s – (panel E). Galvanostatic charge-discharge (GCD) curves of GNRs and GNRs-300 at various current densities – (panel F and G). Variation in the value of C_s obtained from the GCD curves for different current densities – (panel H). GCD curves of GO (mass loading 0.004 mg (0.057 mg/cm²)), GNRs and GNRs-300 at a current density of 1

A/g – (panel I). Variation in the C_s and coulombic efficiency as a function of number of cycles (panel J) and the GCD curves for the first and last three cycles – (panel J-inset). All electrochemical measurements were performed in 1 M H_2SO_4 as an aqueous supporting electrolyte.

Fig. 12A shows the change in energy density for the as synthesized GNRs and GNRs-300 at various current densities. Fig. 12B shows the Ragone plot for GNRs and GNRs-300 exhibited the high energy density of 26.76 Wh/kg and 21.95 Wh/kg at a power density of 400 W/kg, respectively. Under identical experimental conditions the value of energy density for GRH was found to be 19.55 Wh/kg. Notably, even at a higher power density of 5944 W/kg, the energy density for GNRs decreased to 16.84 Wh/kg only. These results evidently suggest the tremendous potential of the as synthesised GNRs as electrode material in energy storage devices.

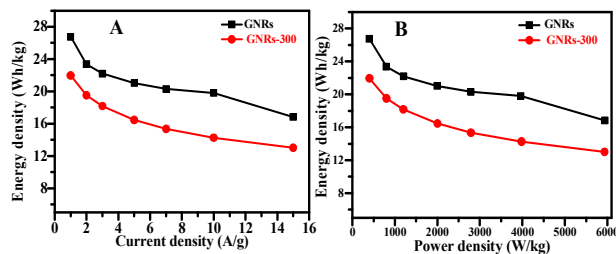


Fig. 12 Change in energy density of GNRs and GNRs-300 electrode in aqueous electrolyte with current density (A) and Ragone plot for GNRs and GNRs-300 (B).

Discussion

The reduction of GO to reduced graphene oxide using malonic acid as a reductant at pH 6.0 was confirmed by the optical absorption spectroscopy and XRD (Figs. 1 and 2). It was exciting to observe that reduction of GO at pH 6.0 results in the formation of GNRs (Figs. 3-5), unlike to that at pH(s) \sim 7.5 and 10.5, which produced stacked aggregated GNRs (Fig. S6, ESI⁺) and ultrathin graphene sheets, respectively.²⁶ A further lowering in pH than 6.0, however, caused this solution to undergo aggregation possibly because of relatively lesser negative ζ -potential. It may be mentioned that for pH(s) (\geq 8) the reduction of GO result in the formation of graphene sheets only (not shown). These observations suggest that the pH of the solution plays a crucial role in the formation of carbon nanostructures with different morphologies. In control experiments, the reduction of GO was also investigated at pH 6.0 at 95 °C without using any additional reducing agent (GRL-OH⁻) as well as by employing oxalic acid as reducing agent (GRL-Ox), which did not contain active methylene group unlike malonic acid used in the present work. At pH 6.0 in the absence of additional reducing agent, the absorption spectrum obtained even after 10 h of reaction exhibited the absorption maximum at 253 nm (Fig. S7, ESI⁺). Under similar experimental conditions, the use of oxalic acid as reductant for GO showed the absorption maximum at 258 nm (Fig. S8, ESI⁺). However, the complete reduction of GO by oxalic acid was observed to take place in about 15 h (Fig. S9, ESI⁺). These experiments clearly reveal the reduction of GO with malonic acid containing active methylene group to be more effective as compared to that of OH⁻ and oxalic acid. It thus suggests the present approach to be the most effective wet chemical method

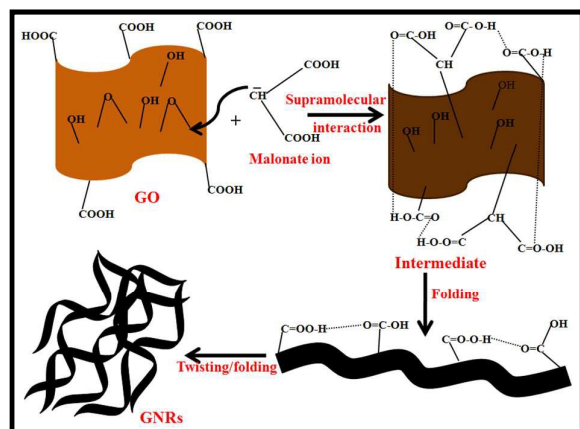
producing GNRs from GO in a single step under mild conditions.

In Raman spectroscopy an increase in the intensity of D band (I_D/I_G ratio) and the presence of D' band (Fig. 7) suggests the existence of defects in GNRs, which might have arisen possibly due to the presence of edges,¹⁵ structural disorder/residual functionalities (Fig. 7). As synthesized GNRs had a thickness of about 3.3 ± 0.2 nm (Fig. 3) and were found to be \sim 0.15 to 1 mm long (Fig. S3, ESI⁺) having a width varied between \sim 150 - 300 nm (Fig. 5), as was revealed by AFM, FESEM and TEM analyses, respectively.

The formation of GNRs at pH 6.0 can be analyzed in terms of the pK_a (s) of malonic acid (2.83 and 5.69), which suggest that at this pH the carboxyl groups (-COOH) of malonic acid are partially unionized (Fig. S10, ESI⁺). It was also evidenced by ζ -potential measurements at pH 6.0, which shows relatively less negative ζ -potential (-45 mV) as compared to that of at pH 10.5 (-55 mV).²⁶ Obviously, the equilibrium between different resonating structures remains shifted towards unionized form (Fig. S10, ESI⁺).

GO exhibits the formation of sheet like structure having various oxygen functionalities like hydroxyl, epoxide and carboxyl groups, which in the presence of malonic acid at pH 6.0 is reduced to form GNRs with relatively much lesser residual functionalities (mainly carboxylic groups) as was evidenced by IR, XPS and solid state ¹³C MAS-NMR studies (Figs. 6, 8 and 9). The difference in the morphology at pH 6.0, compared to that of pH 10.5²⁶, possibly arises because of the formation of an intermediate(s) between GO and malonic acid that might have caused its folding to form the nanoribbon like structure (Scheme 1). It is anticipated to occur through supramolecular interactions involving -COOH groups of malonic acid and residual -COOH groups on various edges of the reduced GO. The growth of the carbon nanostructures then takes place through weak non-covalent interactions in the process of self-assembly involving several such micron-sized intermediates produced from reduced GO. It leads to their folding and eventually results in the formation of \sim 0.15 to 1 mm long curled GNRs. The folding of sheet by AFM was also apparent by an increase in the thickness to 3.3 ± 0.2 nm in the present work as compared to that of sheet observed earlier at pH 10.5 (0.41 ± 0.03 nm).²⁶

The significant reduction in the intensity of C-OH and O=C=O functionalities and complete elimination of C-O-C and ketonic C=O groups in GNRs is clearly evidenced by solid state ¹³C MAS NMR (Fig. 9). These findings are in accordance with the XPS data (Fig. 8). On the contrary, solid state ¹³C MAS NMR spectrum of GNRs-300 exhibits almost complete removal of oxygen containing groups (C-OH and O=C=O), which is understood by the removal of residual functionalities on GNRs (Fig. 9). This observation is also supported by its IR spectrum (Fig. 6). This aspect is manifested by the morphological changes observed by FESEM and TEM images of GNRs-300, which indicated the straightening of the folded GNRs and can be explained by the decreased extent of supramolecular interaction through -COOH groups (Figs. 4 and 5). AFM analysis of GNRs-300, in which the surface height was reduce to 1.1 ± 0.5 nm as compared to those of GNRs (3.3 ± 0.2) (Fig. 3), evidently validates the removal of remaining functionalities on GNRs. This is also indicated by the significant increase in the BET surface area of GNRs-300 (470 m²/g) as compared to that of GNRs (129 m²/g).



Scheme 1 Scheme showing the nucleophilic attack of malonate ion on the epoxy group of GO and resulting in the formation of graphene nanoribbons (GNRs).

The annealing of GNRs at a mild temperature of 300 °C (GNRs-300) also resulted in the development of crystallinity in GNRs-300, as was evidenced by its XRD, SAED and HRTEM analyses (Figs. 2 and 5). The extent of reduction of GO to GNRs and GNRs-300 is also indicated by the I-V measurements which showed more than four orders of magnitudes higher conductivity for GNRs (2.85 S/cm) as compared to that of GO (2.7 × 10⁻⁴ S/cm) (Fig. 10) confirming the restoration of sp² character in GNRs upon reduction. Interestingly, the conductivity for GNRs-300 (14.7 S/cm) is more than five times to that of GNRs, which clearly demonstrates that the annealing further enhances the sp² character in as synthesized GNRs at a mild temperature of 300 °C (Fig. 10). A linear dependence in I-V curves in these cases suggests the as synthesized GNRs / GNRs-300 display metallic behavior. The observed ohmic behavior indicates it to have sp² hybridized domain.³⁷ The value of current in the entire recorded range of voltage is more than an order of magnitude higher to those reported for reduced GO obtained by thermal exfoliation and reduction of GO at a much higher temperature (1100 °C).³⁷

In the present case the shape of the CV curves for GNRs evidently suggests that the specific capacitance (C_s) (122 F/g at 100 mV/s) is largely contributed due to EDLC involving non-faradic storage of charge through reversible adsorption of ions. A partial contribution to the C_s also arises owing to pseudo-capacitance involving faradic reaction due to residual oxygen functionalities on GNRs at the edge planes, as evidenced by IR, XPS and ¹³C NMR (Figs. 6, 8 and 9), and H⁺ ions of electrolyte (Fig. 11B). In addition to this the hydrophilic nature of the residual functionalities on GNRs might facilitates the increased permeability of electrolytic solution, resulting in the faster wetting of the electrode,^{38,39} contributing to the C_s. The observed decrease in C_s value for GNRs-300 (91 F/g at 100 mV/s) can be attributed to the loss in pseudo-capacitive functionalities from the edge plane(s) of GNRs (Fig. 11 C) as is reflected by the increase in conductivity arising mainly due to EDLC.

The C_s value of as synthesized GNRs, measured from GCD curves (301 F/g at 1 A/g) (Fig. 11F), is fairly high in comparison to that of GRH (220 F/g at 1 A/g), as well as graphene sheets synthesized by employing various other reducing agents such as: Sn powder (152 F/g at 1.5 A/g), trigol (130 F/g at 1 A/g), tartaric/malic / oxalic acid (100.8/112.4/147 F/g at 0.1 A/g), caffeic acid (136 F/g at 1 A/g) and from bio-reduction (137 F/g at 1.3 A/g);

and even higher to those of some N doped graphene sheets employing reducing agents such as: hydrazine (133 F/g at 1 A/g) and ammonia (233.3 F/g at 0.5 A/g).⁴⁰⁻⁴⁶ For GNRs synthesized by electrochemical exfoliation of graphite using aqueous electrolyte the C_s value was found to be (140 F/g at 1 A/g).⁴⁷ Whereas, for GNRs synthesized by unzipping of pristine MWCNTs / CNTs varied values of C_s were obtained based on the method were as follows: employing H₃PO₄ as reducing agent (150 F/g at 1A/g)⁴⁸; using hydroiodic acid as reductant (147 F/g at 0.5 A/g)⁴⁹; heat treatment in Ar at 600 °C of: oxidized CNTs (130 F/g at 1 mV/s)⁵⁰ and graphene oxide nanoribbons obtained from MWCNTs (115.6 F/g at 1.7 A/g).⁵¹ Further, the high value of C_s (193 F/g) at current density of 15 A/g after 4000 cycles suggests this system to be fairly stable. Moreover, the energy density (Wh/kg) values for: GNRs (23.36) and GNRs-300 (19.52) calculated at a power density of 800 W/kg (Fig. 12B) are much higher to those reported for thermally reduced graphene oxide nanoribbons (15.06 Wh/kg at 807 W/kg)⁵¹, and are significantly higher to those of the available commercial supercapacitor(s).⁵²

To the best of our knowledge, this is the first report producing nanoribbons of ~ 0.15 to 1 mm long and a few hundred nm wide employing a simple wet chemically controlled approach in aqueous medium using mild reducing agent. Further, the use of mild conditions of pH and temperature for performing the reduction of GO makes it environmental friendly approach for the formation of GNRs. The high aspect ratio (~ 0.15 to 1 mm (l) × ≤ 300 nm (w)) of as synthesized few layer conducting GNRs suggests it viable material for usage in microelectronics and other electronic devices. The enhanced electrochemical behavior of as synthesized GNRs with fairly high value of specific capacitance at high current density in aqueous electrolyte with long term cyclic stability, high coulombic efficiency, and high energy density/power density demonstrates it to have a significant potential for future applications as energy storage electrode material and supercapacitor.⁵³

Conclusions

We have developed for the first time a single step wet chemical synthesis route for the formation of curls shaped graphene nanoribbons (GNRs) entangled with each other using mild reducing agent and experimental conditions. The reduction of GO to GNRs is evidenced by optical, XRD, Raman, IR, XPS and ¹³C MAS NMR. The residual functionalities on GNRs is revealed by IR, XPS and ¹³C MAS NMR, which assisted in the process of the growth of carbon nanostructures to yield GNRs involving weak non-covalent bonding. AFM analysis indicates the formation of a few layer GNRs and annealing reduces its thickness to about 1/3rd, which is also manifested by more than 3.5 times increase in surface area of GNRs-300 as compared to that of GNRs. The removal of residual functionalities upon annealing at mild temperature of 300 °C (GNRs-300), associated with the development of polycrystallinity, results in their unfolding due to reduction in supramolecular interactions. Solid state ¹³C MAS NMR spectra clearly confirms the increasing graphitic character following the order: GO < GNRs < GNRs-300 as is also evidenced by I-V analysis exhibiting the same order for the increase in conductivity. GNRs modified electrode material exhibiting high: specific capacitance, cycling ability, coulombic efficiency and energy density/power density clearly demonstrate the as

synthesized GNRs to have tremendous potential for supercapacitor applications.

Experimental Section

Reagents and Materials

The chemicals - natural graphite flakes (75 + mesh) (Aldrich); malonic acid, hydrogen peroxide (30%), potassium permanganate, P₂O₅ and hydrochloric acid (s-d Fine chemicals Ltd.); dimethylformamide (DMF), K₂S₂O₈ (Merck); oxalic acid (Rankem); sulphuric acid (Thomas Baker 98%); sodium hydroxide pellets (Himedia); dialysis tubing (seamless cellulose tubing and dialysis tubing closures) (Sigma). All the reagents were of analytical grade and used as received without any further purification. Fresh Millipore water was used for the preparation of solutions (Bedford, MA, USA).

Equipment

Optical absorption spectra were recorded in the UV-Visible range (200 – 800 nm) on a Shimadzu UV2100 spectrophotometer using a quartz cuvette having a path length of 1 mm. Zeta potential (ζ) measurement was carried out on a Malvern Instruments, Nano-ZS90 (Zetasizer Nanoseries) equipped with a He - Ne laser (632 nm) as the light source. X-ray diffraction patterns were recorded on a Bruker AXS D8 Advance X-ray diffractometer (XRD) in the 2 θ range of 7 to 50° at a scan rate of 0.2°/step using Cu K α radiation (1.5418 Å) at a voltage and current of 40 kV and 30 mA, respectively. Atomic force microscope (AFM, NTEGRE (NT-MDT)) equipped with NOVA software in a semi-contact mode was used to study the surface topography of the samples by recording two-dimensional images. It has a resolution of 0.2 nm along x and y axes and 0.04 nm along z axis. Surface morphologies were also analyzed by using digital field emission scanning electron microscope (FE-SEM) QUANTA 200-FEG equipped with charged-coupled device (CCD) camera. Elemental analyses at different locations and mapping of the FESEM images were performed by using energy dispersive x-ray analysis (EDAX) accessories from AMETEK materials analysis division equipped with Aztec energy analysis software. Transmission electron micrographs (TEM), high resolution transmission electron micrographs (HRTEM) and selected area electron diffraction (SAED) measurements were obtained on a FEI- Tecnai G2 20 S-TWIN at an operating voltage of 200 kV equipped with CCD camera having different magnifications up to 110000 X. It has a point and line resolution of 0.24 and 0.14 nm, respectively. Raman measurements were carried out on Renishaw inVia Raman spectrometer (serial no. 021R88) equipped with argon ion laser (514 nm), confocal microscope with different objective lenses and CCD detector. Infrared spectra were recorded on a Thermo Nicolet Nexus Fourier transform infrared (FTIR) spectrophotometer in the mid IR range of 4000 - 400 cm⁻¹ in KBr medium and were processed by using OMNIC v6.1 software. X-ray photoelectron spectroscopy (XPS) measurements were recorded on an Omicron nanotechnology instrument using an Al K α energy source (1486.6 eV) and custom built ambient pressure photoelectron spectrometer (Lab-APPES) (Prevac, Poland) equipped with VG Scienta's R3000HP analyzer and Al K α monochromator (MX650), respectively. The solid-state direct ¹³C single pulse magic angle spinning (MAS) nuclear magnetic resonance (NMR) spectra were recorded on a JEOL 400 MHz NMR spectrometer (Model ECX 400 II). The samples were packed into 4 mm rotor and spun at 12 kHz. The spectra were averaged for more than 3000 scans using 10 s relaxation delays and 2.4 μ s 90° pulse exciting over a bandwidth of 100 MHz without decoupling. Solid adamantane (29.4 ppm) was

used as the reference for ¹³C spectrum based on trimethylsilane scale. Current- voltage (I-V) measurements were performed on the equipment supplied from Photo Emission Tech. Inc., USA equipped with Keithley 2400 source meter at room temperature using four probe method. N₂ sorption isotherms were recorded at 77 K using Autosorb-iQ (Quantachrome Instruments). Cyclic voltammetry (CV) and galvanostatic charge-discharge (GCD) measurements were performed on a computer controlled CHI760E electrochemical workstations (CH Instruments, USA) using a three electrode configuration. Glassy carbon electrode (GCE) of 3mm diameter (0.07065 cm² area) was employed as a working electrode, Pt wire as a counter electrode and Ag/AgCl (3M NaCl) as a reference electrode. All the electrochemical measurements were performed in 1M H₂SO₄ as an aqueous supporting electrolyte. Refrigerated circulating water baths from Lab companion (Model RW- 0525G and 1025G) were used for performing the reactions at 95 °C. Toshnival digital pH meter (Model CL 54 +) was used for maintaining the pH of the solutions. The samples were centrifuged by using REMI microprocessor research compufuge (Model PR-24) at a centrifugation speed of 13000 rpm and were dried in a vacuum oven from Labtech, Daihan Labtech Co. Ltd. Annealing of the samples were carried out in air using Metrex high temperature furnace equipped with microprocessor temperature controller.

Methodology

For Raman measurements, the small amount of solid sample was placed on the clean glass substrate underneath the 50X objective lens having spectral resolution of 0.5 - 1 cm⁻¹ in Raman shift and these samples were recorded in the spectral range of 500 - 3500 cm⁻¹. All spectra were measured at low laser power of 0.5 mW for an exposure time of 30 s in order to avoid any damage to the samples. The calibration was made using silicon reference at 520 cm⁻¹. For AFM analysis, samples were prepared by dispersing the small amount of solid sample in de-ionised water. A drop of this solution was applied on the glass substrate, which was dried under ambient conditions. AFM images were recorded by varying the scanning frequency in the range of 1.56 to 3.13 Hz at room temperature. From the AFM images of the sample, the surface height was measured along a particular line by using NOVA software. For FESEM analysis, samples were prepared by mounting the small amount of solid sample on the double sided tape, which is fixed on the aluminium stub. The surface of these samples was sputtered with gold in order to make them conducting and then the images were recorded by applying an acceleration voltage of 20 kV. For TEM analysis, samples were prepared by sonicating the small amount of solid sample in deionised water for about 15-20 min and then a drop of this solution was applied on a carbon coated copper grid G-200 (size 3.05 mm). The grid was subsequently dried in dark to evaporate the remaining moisture prior to its analysis at room temperature. For N₂ sorption measurements, the samples were degassed at 120 °C for about 12 h under vacuum prior to its analysis. Specific surface area, average pore diameter and pore size distribution was analyzed from Brunauer–Emmett–Teller (BET) equation and density functional theory (DFT) method, respectively by using Nova Win software. For I-V measurements, the film was prepared by applying the drop of liquid sample on a transparent conducting indium titanium oxide substrate. The electrical contacts were made by using silver paste. The resistivity was calculated by using the below given equation (1):

$$\rho = \left(\frac{\pi l}{\ln 2} \right) \left(\frac{V}{I} \right) \quad (1)$$

Where, ρ (Ω cm) is the resistivity, t (cm) is the thickness of the samples, V (V) is the applied potential and I (A) is the current flowing through the material. The conductivity (σ) can be calculated using $\sigma = 1/\rho$ (S/cm). The thickness of the samples was determined to be 4, 6 and 5 μm for GO, GNRs and GNRs-300, respectively. Specific capacitance (C_s) (F/g) from CV curves was calculated by using the below given equation 2³⁹:

$$\frac{1}{2m \cdot \Delta V \cdot s} \left(\int_{0.8}^0 idV + \int_0^{0.8} idV \right) \quad (2)$$

Where, m (g) is the mass of the material applied on the electrode, ΔV (V) is the change in potential window and s

(mV/s) is the scan rate and $\int_{0.8}^0 idV + \int_0^{0.8} idV$ (A) is the total

current obtained by the integration of positive and negative sweep in cyclic voltammetry. C_s from GCD curves was calculated by using the below given equation 3⁴⁰:

$$C_s = \frac{I \cdot \Delta t}{\Delta V \cdot m} \quad (3)$$

Where, I (A) is the discharging current, Δt (s) is the discharging time, ΔV (V) is the potential change during discharging step and m (g) is the mass of the active material. The CV and GCD measurements were performed in the same potential window of 0.0 - 0.8 V. Coulombic efficiency (η) of GNRs modified electrode was calculated from long cycle GCD curve at 10 A/g by using the below given equation 4⁵³:

$$\eta = \frac{T_d}{T_c} \times 100 \% \quad (4)$$

Where, η is the Coulombic efficiency, T_d and T_c is the discharging and charging time, respectively. The η was calculated from 1st to 1000th cycle after every 100th cycle.

Energy densities and power densities of GNRs electrode at different current densities using GCD measurements were calculated by using the below given equations 5 and 6, respectively⁵⁰:

$$E = \frac{C_s \Delta V^2}{2 \times 3.6} \quad (5)$$

$$P = \frac{E \times 3600}{t} \quad (6)$$

Where, C_s (F/g) is the specific capacitance at different current densities, ΔV (V) is the potential window, E (Wh/kg) is the energy density, P (W/kg) is the power density and t (h) is the discharging time.

The samples were dried in a vacuum oven at 50 $^{\circ}\text{C}$ for 12 h and were used as such for the measurements of XRD, FTIR, XPS and ^{13}C MAS NMR. For BET analysis, pellets of about 1-2 mm thickness were prepared using hydraulic press by applying a pressure of about 11 tons.

Synthesis of Graphene Oxide (GO)

GO was synthesized from natural graphite flakes following the modified Hummers method as discussed earlier.^{54,26} The solid GO thus obtained was diluted to make its dispersion in deionised water (DIW) (5 mg/mL). This GO dispersion was then dialyzed for one week to remove any remaining metal species. Out of this, 0.5 mg/mL of dispersion was exfoliated into DIW by sonication under ambient conditions for 30 min. The resulting homogeneous yellow

brown dispersion was stable for several months and was employed further for performing reduction.

Synthesis of Graphene Nanoribbons (GNRs)

The chemical reduction of GO into GNRs was performed by using malonic acid as a reducing agent. The completion of the reaction was adjudged by noting a change in the color from yellow-brown to homogenous black and monitoring the change spectrophotometrically. The ratio of the amount of GO to malonic acid and the heating time of the reaction mixture was optimized by varying the amount of GO: malonic acid from 1: 1.2 - 5.2 and 1 to 12 h, respectively. The maximum amount of the product was obtained for: GO: malonic acid ratio and time of heating to be 1: 3.2 and 10 h, respectively at pH 6.0. Further heating of this reaction mixture did not cause any change in the optical spectrum. The optimized sample was prepared by mixing of 40 mg malonic acid into 25 mL of GO dispersion (0.5 mg/mL) under vigorous stirring and the pH of this reaction mixture was maintained at 6.0 by using dilute NaOH. The resulting solution was heated in a circulating water bath for 10 h at 95 $^{\circ}\text{C}$. The resulting black suspension was repeatedly washed with DIW for about eight to nine times in order to remove any unreacted malonic acid and was separated each time by centrifugation. The product thus obtained was dispersed into DIW at a pH of 6.0 and has been denoted as GNRs. Annealing of the as synthesised GNRs was carried out at 300 $^{\circ}\text{C}$ and it has been denoted as GNRs-300. In a control experiment reduced graphene oxide was synthesized by using the same amount of malonic acid as used in the present work, but its pH was maintained at 10.5 and is denoted as GRH.

Modification of working electrodes

The GCE electrodes were polished sequentially by alumina powder of size 1 μm followed by 0.5 and 0.03 μm using microcloth pad. The electrodes were rinsed thoroughly in an ultrasonic bath sequentially using DIW and ethanol for about 10 - 15 min, respectively. GCE electrodes were then dried under the flow of N_2 . GNRs dispersion was prepared by suspending it in DMF (0.5 mg/mL) by ultrasonication for about 20-30 min without adding any binder^{41, 55,56}, as it might influence the electrochemical behaviour of the electrode material.⁵² This homogeneously prepared solution (30 μL) was drop-casted repeatedly after drying each time onto the surface of GCE electrode. The electrode surface was then allowed to dry overnight at room temperature. The loading mass on the working electrode for GNRs, GNRs-300 and GRH was kept at 0.015 mg (0.21 mg/cm²), which was also verified by weighing the electrode before and after loading of the sample using ultrasensitive METTLER-TOLEDO balance. Similar procedure was adopted for the preparation of GO modified working electrode with the mass loading of 0.015 mg (0.21 mg/cm²) for CV measurements. The electrolyte (1 M H_2SO_4) was purged strongly with N_2 for about 5 min in order to remove any dissolved oxygen prior to performing electrochemical measurements.

Acknowledgements

Mahima Khandelwal is thankful to MHRD, New Delhi for the award of SRF. Thanks are also due to Head, IIC, IIT Roorkee, Roorkee for providing the facilities of FE-SEM, TEM and AFM.

References

- F. Schwierz, *Nat. Nanotechnol.*, 2010, **5**, 487.
- X. Li, Y. Zhu, W. Cai, M. Borysiak, B. Han, D. Chen, R. D. Piner, L. Colombo and R. S. Ruoff, *Nano Lett.*, 2009, **9**, 4359.
- C. Lee, X. Wei, J. W. Kysar and J. Hone, *Science*, 2008, **321**, 385.
- A. Ambrosi, C. K. Chua, A. Bonanni and M. Pumera, *Chem. Rev.*, 2014, **114**, 7150.
- Y. Wang, Z. Li, J. Wang, J. Li and Y. Li, *Trends Biotechnol.*, 2011, **29**, 205.
- S. L. Candelaria, Y. Shao, W. Zhou, X. Li, J. Xiao, J.-G. Zhang, Y. Wong, J. Liu, J. Li and G. Cao, *Nano Energy*, 2012, **1**, 195.
- S. Bose, T. Kulia, A. K. Mishra, R. Rajasekar, N. H. Kim and J. H. Lee, *J. Mater. Chem.*, 2012, **22**, 767.
- Y. Gong, H. Fei, X. Zou, W. Zhou, S. Yang, G. Ye, Z. Liu, Z. Peng, J. Lou, R. Vajtai, B. I. Yakobson, J. M. Tour and P. M. Ajayan, *Chem. Mater.*, 2015, **27**, 1181.
- Z. Chen, Y.-M. Lin, M. J. Rooks and P. Avouris, *Physica E*, 2007, **40**, 228.
- A. Martin, J. Hernández-Ferrer, L. Vázquez, M.-T. Martínez and A. Escarpa, *RSC Adv.*, 2014, **4**, 132.
- V. Georgakilas, M. Otyepka, A. B. Bourlinos, V. Chandra, N. Kim, K. Christian, P. Hobza, R. Zboril and K. S. Kim, *Chem. Rev.*, 2012, **112**, 6156.
- M. Y. Han, B. Özyilmaz, Y. Zhang and P. Kim, *Phys. Rev. Lett.*, 2007, **98**, 206805.
- L. Tapasztó, G. Dobrik, P. Lambin and L. P. Biró, *Nat. Nanotechnol.*, 2008, **3**, 397.
- Z.-S. Wu, W. Ren, L. Gao, B. Liu, J. Zhao and H.-M. Cheng, *Nano Res.*, 2010, **3**, 16.
- J. Campos-Delgado, J. M. Romo-Herrera, X. Jia, D. A. Cullen, H. Muramatsu, Y. A. Kim, T. Hayashi, Z. Ren, D. J. Smith, Y. Okuno, T. Ohba, H. Kanoh, K. Kaneko, M. Endo, H. Terrones, M. S. Dresselhaus and M. Terrones, *Nano Lett.*, 2008, **8**, 2773.
- J. Campos-Delgado, Y. A. Kim, T. Hayashi, A. Morelos-Gómez, M. Hofmann, H. Muramatsu, M. Endo, H. Terrones, R. D. Shull, M. S. Dresselhaus and M. Terrones, *Chem. Phys. Lett.*, 2009, **469**, 177.
- D. V. Kosynkin, A. L. Higginbotham, A. Sinitskii, J. R. Lomeda, A. Dimiev, B. K. Price and J. M. Tour, *Nature*, 2009, **458**, 872.
- L. Jiao, L. Zhang, X. Wang, G. Diankov and H. Dai, *Nature*, 2009, **458**, 877.
- L. Jiao, X. Wang, G. Diankov, H. Wang and H. Dai, *Nat. Nanotechnol.*, 2010, **5**, 321.
- L. Ci, Z. Xu, L. Wang, W. Gao, F. Ding, K. F. Kelly, B. I. Yakobson and P. M. Ajayan, *Nano Res.*, 2008, **1**, 116.
- M. Choucair, B. Gong and J. A. Stride, *Mater. Lett.*, 2014, **119**, 75.
- H. A. Wong and M. Pumera, *J. Mater. Chem. C*, 2014, **2**, 856.
- M. Dimiev, A. Gizzatov, L. J. Wilson and J. M. Tour, *Chem. Comm.*, 2013, **49**, 2613.
- A. Gizzatov, A. Dimiev, Y. Mackeyev, J. M. Tour and L. J. Wilson, *Chem. Comm.*, 2012, **48**, 5602.
- Zhang, Q. Ma, H. Fan, H. Yang and S. Liu, *Carbon*, 2014, **71**, 120.
- A. Kumar and M. Khandelwal, *J. Mater. Chem. A*, 2014, **2**, 20345.
- P.-G. Ren, D.-X. Yan, X. Ji, T. Chen and Z.-M. Li, *Nanotechnology*, 2011, **22**, 055705.
- G. Eda and M. Chhowalla, *Adv. Mater.*, 2010, **22**, 2392.
- Y. Feng, N. Feng and D. Guixiang, *RSC Adv.* 2013, **3**, 21466.
- A. Kumar and M. Khandelwal, *New J. Chem.*, 2014, **38**, 3457.
- P. Solís-Fernández, R. Rozada, J. I. Paredes, S. Villar-Rodil, M. J. Fernández-Merino, L. Guardia, A. Martínez-Alonso and J. M. D. Tascón, *J. Alloy Compd.*, 2012, **536S**, S532.
- D. Rosenthal, M. Ruta, R. Schlögl and L. Kiwi-Minsker, *Carbon*, 2010, **48**, 1835.
- W. Gao, L. B. Alemany, L. Ci and P. M. Ajayan, *Nat. Chem.*, 2009, **1**, 403.
- D. Zhang, X. Zhang, Y. Chen, C. Wang and Y. Ma, *Electrochim. Acta*, 2012, **69**, 364.
- Z. Lin, Y. Liu, Y. Yao, O. J. Hildreth, Z. Li, K. Moon and C.-P. Wong, *J. Phys. Chem. C*, 2011, **115**, 7120.
- Y. Lin, Y. Li, M. Zhong, Y. Yang, Y. Wen and M. Wang, *J. Mater. Chem.*, 2011, **21**, 15449.
- C. Punckt, F. Muckel, S. Wolff, I. A. Aksay, C. A. Chavarin, G. Bacher and W. Mertin, *Appl. Phys. Lett.*, 2013, **102**, 023114.
- B. Rajagopalan and J. S. Chung, *Nanoscale Res. Lett.*, 2014, **9**, 535.
- Y. Chen, X. Zhang, D. Zhang, P. Yu and Y. Ma, *Carbon*, 2011, **49**, 573.
- N. H. Kim, P. Khanra, T. Kulia and J. H. Lee, *J. Mater. Chem. A*, 2013, **1**, 11320.
- D. Mhamane, S. M. Unni, A. Suryawanshi, O. Game, C. Rode, B. Hannoyer, S. Kurungot and S. Ogale, *J. Mater. Chem.*, 2012, **22**, 1140.
- X. Teng, M. Yan and H. Bi, *Spectrochim. Acta Part A* 2014, **118**, 1020.
- Z. Bo, X. Shuai, S. Mao, H. Yang, J. Qian, J. Chen, J. Yan and K. Cen, *Sci. Rep.*, 2014, **4**, 4684.
- M. Jana, S. Saha, P. Khanra, N. C. Murmu, S. K. Srivastava, T. Kulia and J. H. Lee, *Mater. Sci. Eng. B*, 2014, **186**, 33.
- N. Xiao, D. Lau, W. Shi, J. Zhu, X. Dong, H. H. Hng and Q. Yan, *Carbon*, 2013, **57**, 184.
- X. Du, C. Zhou, H.-Y. Liu, Y.-W. Mai and G. Wang, *J. Power Sources*, 2013, **241**, 460.
- D. Damien, B. Babu, T.N. Narayanan, A. L. Reddy, P. M. Ajayan and M. M. Shaijumon, *Graphene*, 2013, **1**, 37.
- M. Liu, W. W. Tjiu, J. Pan, C. Zhang, W. Gao and T. Liu, *Nanoscale*, 2014, **6**, 4233.
- M. Liu, Y.-E. Miao, C. Zhang, W. W. Tjiu, Z. Yang, H. Peng and T. Liu, *Nanoscale*, 2013, **5**, 7312.
- C. Zheng, X. F. Zhou, H. L. Cao, G. H. Wang and Z. P. Liu, *J. Mater. Chem. A*, 2014, **2**, 7484.
- V. Sahu, S. Shekhar, R. K. Sharma and G. Singh, *ACS Appl. Mater. Interfaces* 2015, **7**, 3110.
- D. Ghosh, S. Giri, M. Moniruzzaman, T. Basu, M. Mandal and C. K. Das, *Dalton Trans.*, 2014, **43**, 11067.
- P. Khanra, T. Kulia, S. H. Bae, N. H. Kim and J. H. Lee, *J. Mater. Chem.*, 2012, **22**, 24403.
- W. S. Hummers and R. E. Offeman, *J. Am. Chem. Soc.*, 1958, **80**, 1339.
- J. Yang and L. Zou, *Electrochim. Acta*, 2014, **130**, 791.
- S. A. El-Khodary, G. M. El-Enany, M. El-Okri and M. Ibrahim, *Electrochim. Acta*, 2014, **150**, 269.

Graphical Abstract

One-step chemically controlled wet synthesis of graphene nanoribbons from graphene oxide for high performance supercapacitor applications

Mahima Khandelwal and Anil Kumar*

Department of Chemistry, Indian Institute of Technology Roorkee, Roorkee - 247667, India

Chemically controlled GO reduction produces (150-300 nm wide and ~0.15 - 1 mm long) GNRs displaying high-performance supercapacitor applications.

